**Key Points:**

- We show the existence of criticality in geomagnetic field data between 6 and 45 hr before the strongest magnetic storms of solar cycle 24
- The dynamics of the magnetosphere prior to storms is analogous to the dynamics of thermal systems undergoing second-order phase transition
- Space weather forecasting schemes could take into account these findings and implement them as potential precursors of storm activity

**Correspondence to:**
G. Balasis,
gbalasis@noa.gr

# Observation of Intermittency-Induced Critical Dynamics in Geomagnetic Field Time Series Prior to the Intense Magnetic Storms of March, June, and December 2015

**Georgios Balasis**[1] , **Ioannis A. Daglis**[1,2] , **Yiannis Contoyiannis**[3] , **Stelios M. Potirakis**[3] , **Constantinos Papadimitriou**[1] , **Nikolaos S. Melis**[4] , **Omiros Giannakis**[1] , **Athanasios Papaioannou**[1] , **Anastasios Anastasiadis**[1] , and **Charalampos Kontoes**[1]

[1]Institute for Astronomy, Astrophysics, Space Applications and Remote Sensing, National Observatory of Athens, Athens, Greece, [2]Department of Physics, National and Kapodistrian University of Athens, Athens, Greece, [3]Department of Electrical and Electronics Engineering, University of West Attica, Athens, Greece, [4]Institute of Geodynamics, National Observatory of Athens, Athens, Greece

**Abstract** Criticality has been proposed as a suitable framework to study the nonlinear system of the Earth's magnetosphere. The magnetic field variations observed by the midlatitude HellENIc GeoMagnetic Array with respect to the most intense magnetic storms (Dst $< -150$ nT) of the current solar cycle (i.e., 17 March, 23 June, and 20 December 2015) are analyzed using the method of critical fluctuations. We show that the application of method of critical fluctuation to the HellENIc GeoMagnetic Array time series reveals the existence of intermittency-induced criticality in the range of 6 to 45 hr prior to the onset of these events. The results suggest that the underlying dynamical processes in the magnetosphere prior to intense magnetic storms present dynamics analogous to those of thermal systems undergoing second-order phase transition. Our findings demonstrate that the proposed method can be very relevant for the analysis of critical fluctuations in the framework of space systems.

## 1. Introduction

The Earth's magnetosphere corresponds to a nonlinear driven dynamical system (Klimas et al., 1996). Among others, Tsurutani et al. (1990) observed indications for a nonlinear behavior of the auroral electrojet (AE) index in response to changes of the interplanetary magnetic field southward component, triggering an intense debate on low-dimensional chaos in magnetospheric dynamics (Baker et al., 1990; Sharma et al., 1993; Vassiliadis et al., 1990; Vörös et al., 2003). Specifically, Chang (1992) suggested that the magnetosphere is a nonlinear system of infinite dimensions that operates near criticality. This hypothesis was further supported by cellular automata models of the AE index (Consolini, 1997) and auroral Ultraviolet Imager observations from the Polar spacecraft (Lui et al., 2000).

In situ observations provided evidence for turbulence and intermittency in plasma sheet (e.g., Angelopoulos et al., 1999). Moreover, the concept of self-organized criticality has been adopted in the investigations of the coupled solar wind-magnetosphere system (Freeman et al., 2000; Uritsky & Pudovkin, 1998) in order to understand its global energy storage and release (Chapman et al., 1998) and the mechanisms of magnetotail dynamics (Consolini, 2002). Sitnov et al. (2001) provided some evidence for phase transitions in the magnetosphere associated with substorm occurrence. The findings by Wanliss (2005) and Balasis et al. (2006, 2008, 2009) indicated the existence of two different regimes in the magnetosphere associated with the prestorm activity and magnetic storms, while Wanliss and Dobias (2007) suggested that the hourly Disturbance storm time (Dst) index variations between quiet and storm times are consistent with nonequilibrium phase transition-style dynamics.

Phase transition phenomena are a very important field in statistical physics, while in the framework of modern complex theories they have found application to almost all sciences. A phase transition phenomenon is characterized by the transition between two phases (states) in which a system could exist. Phase transitions

can be either dramatic, taking place in an abrupt and discontinuous way, termed first-order (e.g., melting, boiling, and sublimation), or smooth, transforming itself into the new phase in a continuous manner, termed second-order (e.g., conducting-superconducting transition in metals at low temperatures). During a phase transition of a given system certain properties of the system change as a result of the change of some external condition (termed control parameter) such as temperature, pressure, or others (e.g., Huang, 1987). As the Earth's magnetosphere evolves toward a magnetic storm, it experiences different states, since different mechanisms are gradually involved in the magnetic storm preparation process. Therefore, in principle, the theory of phase transitions can be conceptually used to describe the changes occurring in the state of the Earth's magnetosphere as gradually evolves from the "normal" or quiet times to "pathological" or storm times under the influence of the solar wind drivers such as interplanetary magnetic field components, dynamic pressure, and velocity.

It is reminded (e.g., Huang, 1987) that in a second-order phase transition the second-order derivative of the thermodynamic free energy (the energy of a system that is available to perform thermodynamic work) is discontinuous while the first-order one is continuous and therefore second-order phase transition is characterized by a gradual change. On the other hand, in a first-order phase transition the first-order derivative of the thermodynamic free energy is discontinuous, and thus, it is characterized by abrupt changes. The so-called "tricritical point" is the point in the phase diagram of the system at which the two aforementioned basic kinds of phase transition meet (e.g., Contoyiannis et al., 2015). Of great interest is the case of the critical point during a second-order phase transition; for a given value of the aforementioned control parameter the system reaches critical state. At the critical state self-similar structures appear both in time and space. This fact is quantitatively manifested by power law expressions describing the distributions of spatial or temporal quantities associated with the aforementioned self-similar structures (Contoyiannis & Diakonos, 2007, Sornette, 2004, Stanley, 1987, 1999). It is clarified that although multiscale nature, that is, the scale invariance or self-similarity, is always a feature of critical state, the vice versa is not valid. This means that if a power law results from the analysis of a time series using an arbitrarily selected method this does not necessarily mean that the system is in critical state. Specifically designed time series analysis methods, such as the here employed method of critical fluctuations (Contoyiannis & Diakonos, 2000, Contoyiannis et al., 2002), are necessary in order to identify a critical state.

The outburst of a magnetic storm itself, that is, the specific extreme event of the sudden lowering of the geomagnetic field values, is apparently an out of equilibrium change of magnetosphere's state. As already mentioned, Wanliss and Dobias (2007) suggested that the Dst index variations between quiet and storm times are consistent with nonequilibrium phase transition-like dynamics. Consequently, the analysis of geomagnetic field time series during the outburst of a magnetic storm is not expected to reveal indications of second-order phase transition. However, during the quiet period preceding the outburst of the magnetic storm the long-scale variations of the geomagnetic field are so slow that do not exclude the possibility that characteristics of a second-order phase transition might be locally embedded in the associated time series.

In this article, we investigate the possibility that one of the early stages of the preparation of three specific intense magnetic storms (Dst < −150 nT), which took place in 2015, could present common characteristics with a thermal system undergoing a second-order phase transition. Specifically, we investigate the possible existence of intermittency-induced critical dynamics in the small-scale (fast) variations of ground-based geomagnetic field measurements during the quiet period a few days to a few hours prior to the onset of these events, using the method of critical fluctuations. Note that method of critical fluctuations has been specifically designed for the analysis of the order parameter fluctuations in thermal systems for the identification of the possible existence of intermittency-induced criticality (or criticality by intermittent dynamics), as well as of the identification of the departure from the critical state.

## 2. ENIGMA Data and Magnetic Storms for 2015

The National Observatory of Athens (NOA) operates since the beginning of the present solar cycle in 2008 the HellENIc GeoMagnetic Array (ENIGMA), an array of three midlatitude magnetometer stations located in central and southern Greece. The ENIGMA stations are Klokotos (abbreviated as THL with geographic coordinates 39.5646°N, 22.0144°E), Dionysos (DIO with 38.0779°N, 23.9331°E), and Velies (VLI with 36.7180°N, 22.9468°E). ENIGMA monitors the geomagnetic field variations associated with the occurrence of magnetic storms and magnetospheric ultra-low frequency waves using vector fluxgate magnetometer instruments (for more information see http://enigma.space.noa.gr/). ENIGMA is a SuperMAG contributor (http://supermag.jhuapl.edu/),

a worldwide collaboration of national agencies and organizations, currently operating more than 500 ground-based magnetic stations (Gjerloev, 2009).

Geospace magnetic storms are the most complex phenomena of magnetospheric dynamics, associated with enhancements of the ring current in the inner magnetosphere (e.g., Daglis, 2001). The midlatitude Dst index and its minute version, the SYM-H index, are used as proxies of the ring current strength and, thus, as measures of the intensity of magnetic storms. For our study, we have considered 1-year ENIGMA 1-Hz fluxgate magnetometer data from 2015, that is, during the period when the most intense magnetic storms of solar cycle 24 occurred, thus focusing on the storms of 17 March (with a minimum Dst index value of −223 nT), 23 June ($Dst_{min}$ = −204 nT), and 20 December ($Dst_{min}$ = −155 nT).

Solar cycles last approximately 11 years. The most recent solar cycle, the 24th, has been the weakest in almost 100 years with its peak in early 2014 (Pesnell, 2016). These three events are indeed the most intense geomagnetic storms of solar cycle 24 (Gopalswamy et al., 2015; Liu et al., 2015; Watari, 2017). In principle, weak to moderate geomagnetic storms are considered to result from solar wind High-Speed Streams (HSS) and/or Corotating Interaction Regions (Gonzalez et al., 1999), while major ones are attributed to the Interplanetary counter parts of Coronal Mass Ejections (ICMEs ; Gosling et al., 1991).

All of the storms selected for this study show a multistep development, which underlines their complexity. We employ solar wind signatures (plasma and magnetic field characteristics) to imprint the connections to the parent solar events that controlled the geomagnetic storm intensity and variability at each case. Although, the selected case studies are in essence contrasting cases of how the Coronal Mass Ejections (CMEs) and their resulting ICMEs generate intense geomagnetic storms, a striking characteristic of all three storms is the development of unexpected geoeffective solar wind structures. As a rule, such structures result from combinations of circumstances that can occur and make an event more geoeffective, that is, pileup of events, shock enhancement of southward fields, HSS causing compressions, as well as, interaction of CMEs. All of which make the prognosis of such storms, similar to those at hand in this work, a challenging task.

## 2.1. Geomagnetic Storms, Their Related Solar, and Interplanetary Signatures

Table 1 summarizes the solar (i.e., CME) and the related ICMEs that were identified in the SOHO/LASCO coronographs and the in situ plasma measurements from Wind, respectively. To this end, it provides the characteristics of the CMEs (speed and width), as well as the start, the end time and the transit speed of the ICME as these were identified in the ICME list of Richardson and Cane, available at http://www.srl.caltech.edu/ACE/ASC/DATA/level3/icmetable2.htm. Furthermore, it displays the outputs of the WSA-ENLIL model, that is, the expected arrival time of the shock, driven by the parent CME, at 1 AU. These results were obtained by the Space Weather Database Of Notifications, Knowledge, Information at https://kauai.ccmc.gsfc.nasa.gov/DONKI/. Next, Table 1 provides the timing of the shock at 1 AU as this is inferred by in situ plasma measurements and is listed in the http://ipshocks.fi/. Finally, the start and the end time of the geomagnetic storm (Watari, 2017) together with the minimum Dst per storm is presented in the consequent columns of Table 1.

### 2.1.1. The 17 March 2015 Geomagnetic Storm

The drivers of the 17 March 2015 geomagnetic storm have been debated from the scientific community (Kataoka et al., 2015; Liu et al., 2015; Marubashi et al., 2016; Wang et al., 2016; Wu et al., 2016). The main source of the storm can be traced back to the solar events on 15 March 2015. A Halo CME with a speed of 719 km/s was marked at 01:48 UT on that day. This CME was associated with a long duration C9.1 solar flare from active region (AR) 12297 (S22° W25°) that peaked at 02:13 UT. However, a partial Halo CME was also recorded a day before, on 14 March 2015, and was likely associated with a C2.6 flare from the same active region (S21° W20°) that peaked around 11:55 UT (Liu et al., 2015). Furthermore, a high-speed stream emanated from an extension of the southern polar coronal hole 659 that rotated across the solar meridian on 14–16 March 2015. Figure 1 presents the in situ signatures observed at the Wind/Solar Wind Experiment (Ogilvie et al., 1995) and the Wind/Magnetic Field Investigator (Lepping et al., 1995). A rather complex situation is revealed. The $D_{st}$ profile indicates a two-step geomagnetic storm sequence. The first minima identify itself in the sheath region behind the shock, while the second one results from within the ICME. At this point it is important to note that while a single, ICME interval was identified by several researchers (Gopalswamy et al., 2015; Kataoka et al., 2015; Marubashi et al., 2016; Wang et al., 2016; Wu et al., 2016), Liu et al. (2015) reported on the interaction between the two successive CMEs and further noted the effect of the HSS that compressed the ICME maintaining a relatively strong ejecta magnetic field and a high speed.

**Table 1**
*Summary of the Geomagnetic Storms, Their Related ICMEs, and Their Driving CMEs Presented in This Study*

| | CME | | | | ENLIL | | |
| No | Date | Time | Speed (km/s) | Width (°) | Date | Time | Shock@ 1 AU |
|---|---|---|---|---|---|---|---|
| 1 | 15.03.2015 | 01:48 | 719 | Halo | 17.03.2015 | 11:39 ± 7 hr | 17.03.2015 04:00 |
| 2 | 18.06.2015 | 17:24 | 1,305 | Halo | 21.06.2015 | 09:26 ± 7 hr | 21.06.2015 16:04 |
| 3 | 19.06.2015 | 06:42 | 584 | Halo | 22.06.2015 | 06:04 ± 7 hr | 22.06.2015 05:04 |
| 4 | 21.06.2015 | 02:36 | 1,366 | Halo | 22.06.2015 | 21:43 ± 7 hr | 22.06.2015 18:08 |
| 5 | 22.06.2015 | 18:36 | 1,209 | Halo | 24.06.2015 | 18:18 ± 7 hr | 24.06.2015 13:07 |
| 6 | 16.12.2015 | 09:36 | 579 | Halo | 19.12.2015 | 00:32 ± 7 hr | 19.12.2015 15:38 |

| | ICME | | | | Geomagnetic storm | | |
| No | Start of the ICME | | End of the ICME | | Vtransit (km/s) | Start of the storm | End of the storm | Dst (nT) |
|---|---|---|---|---|---|---|---|---|
| 1 | 17.03.2015 | 13:00 | 18.03.2015 | 05:00 | 800 | 17.03.2015 04:45 | 21.03.2015 15:00 | −223 |
| 2 | | | | | | | | |
| 3 | | | | | | | | |
| 4 | | | | | | | | |
| 5 | 25.06.2015 | 10:00 | 26.06.2015 | 06:00 | 960 | 22.06.2015 18:33 | 24.06.2015 12:00 | −204 |
| 6 | 20.12.2015 | 03:00 | 21.12.2015 | 20:00 | 540 | 19.12.2015 16:17 | 22.12.2015 02:00 | −155 |

*Note.* Column 1 provides the number of the solar (CME) event, columns 2 and 3 present the date and time of CME occurrence, columns 4 and 5 display the plane-of-sky speed (in km/s) and the width (in degrees) of the CME, column 6–9 provide the start and the end data/time of the ICME, column 10 provides the transit speed (in km/s) of the ICME, columns 11 and 12 present the results of the ENLIL simulations for the arrival time of the shock at 1 AU, column 13 gives the actual timing of the shock arrival at 1 AU, as this was identified in the interplanetary data, columns 14–16 provide the start and the end time of the geomagnetic storm, as well as, the minimum Dst value (in nT). CME = Coronal Mass Ejection; ICME = Interplanetary counter parts of Coronal Mass Ejection.

### 2.1.2. The 23 June 2015 Geomagnetic Storm

As the Sun rotated from east to west (E45°-W42°), a sequence of strong solar events was marked on the Sun from 18 to 25 June 2015, with AR 12371 being their prevalent source. In particular, on 18 June 2015 at 17:24 UT a Halo CME with a speed of 1,305 km/s associated with an M3.0 flare (N13° E45°) that peaked at 17:36 UT was marked. Furthermore, on 21 June 2015, at 02:36 UT, another Halo CME with a speed of 1,366 km/s associated with an M2.0 flare (N12° E13°), peaking at 01:42 UT was recorded. The next day, on 22 June 2015 at 18:36 UT, a Halo CME with a speed of 1,209 km/s associated with an M6.5 flare (N13° W05°) peaking at 18:23 UT was reported. Finally, on 25 June 2015 at 08:36 UT, yet another Halo CME with a speed of 1,627 km/s, associated with an M7.9 flare (N10° W42°), peaking at 08:16 UT was spotted. All of these Halo CMEs impinged the Earth's magnetosphere and resulted to a cluster of shocks. The shocks passed Wind (http://ipshocks.fi/) at 16:04 UT on 21 June, 05:04 UT and 18:08 UT on 22 June, and 13:07 UT on 24 June, respectively. Figure 2 illustrates the relevant solar wind measurements from Wind, similar to Figure 1. The ICME boundaries are taken from the online available level 3 data product of the ACE Science Center (list of Richardson and Cane; http://www.srl.caltech.edu/ACE/ASC/DATA/level3/icmetable2.htm). The first shock seems to be driven by the Halo CME of 18 June 2015. The second one was most probably associated with a Halo CME with a speed of 584 km/s that was marked at 06:42 UT on 19 June 2015. The ICME and its preceding shock (the third one, as these are presented in Figure 2) were produced by the Halo CME that was recorded on 21 June 2015 (Liu et al., 2015). The last shock (fourth in a row) that overtook the ICME at 1 AU was associated with the Halo CME of 22 June 2015. As concerns the evolution of geomagnetic storm, the $D_{st}$ time profile (last panel of Figure 2) shows a multistep geomagnetic storm with a global minimum of −204 nT (orange vertical solid line). Upstream of the third shock, the first drop of the $D_{st}$ index is spotted. This is the output of the fluctuating southward field component. The second drop is identified in the sheath region downstream of the third shock, triggered by the southward field. However, the major drop in the $D_{st}$ index is spotted within the ejecta (ICME) and is the result of the southward field, at this time. As a consequence, the 23 June 2015 geomagnetic storm exhibits a multistep development, caused by the southward fields due to amplification by a series of preceding shocks and those within a single ejecta. In principle, the sequence of the strong solar events of this period and the multiple preceding shocks and the corresponding sheaths most probably resulted in the precondition of the magnetosphere that in turn fostered the growth of an intense geomagnetic storm (Liu et al., 2015).
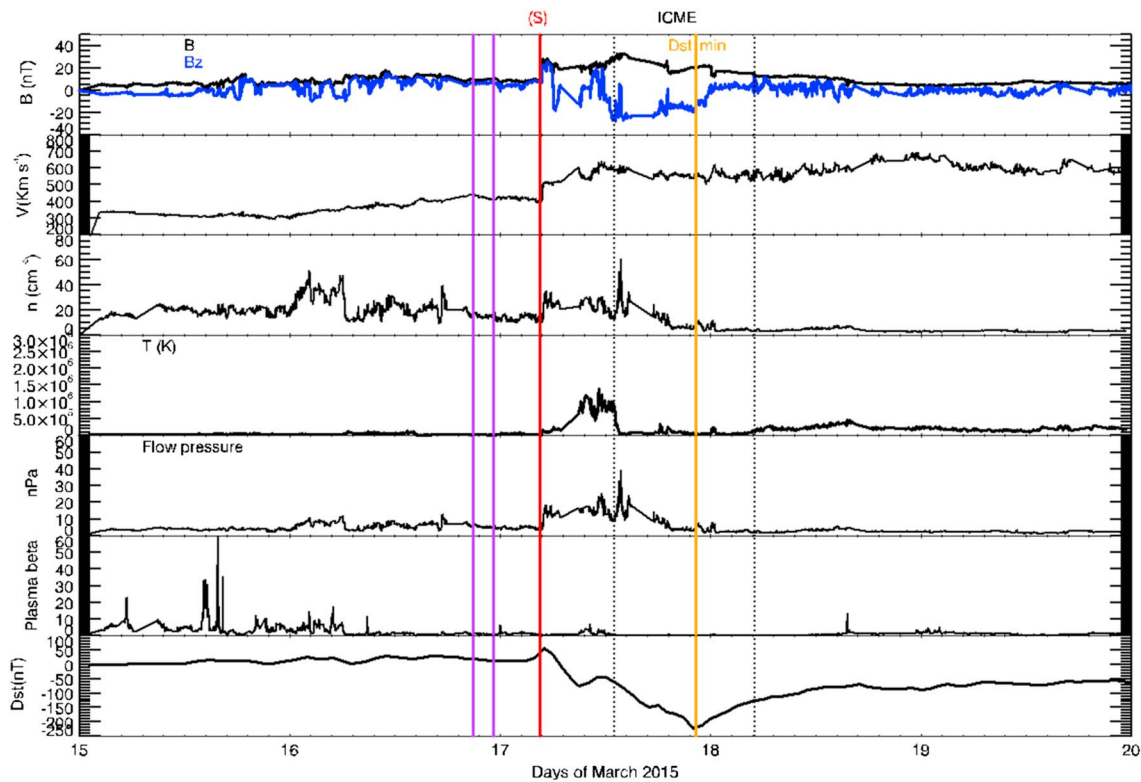
**Figure 1.** From top to bottom the panels present the plasma average magnetic field strength (*B*) and its *Z* component (*B*$_z$); velocity (*V*), proton density (*n*) and temperature (*T*), flow pressure (*P*$_{dyn}$), plasma beta parameter, and the *D*$_{st}$ index respectively for the 17 March 2015 storm. The vertical solid red line indicates the shock passage at Wind taken from http://ipshocks.fi/. The two vertical dotted black lines indicate the start and the end time of the Interplanetary counter parts of Coronal Mass Ejection (ICME), while the solid vertical orange line corresponds to the minimum of the *D*$_{st}$. Moreover, the two vertical purple lines correspond to the time window identified with critical behavior in the HellENIc GeoMagnetic Array time series (16 March 2015, 20:53–23:15 UT), that is, 8 hr prior to the peak of the storm (see also Figure 4).

### 2.1.3. The 20 December 2015 Geomagnetic Storm

On 16 December 2015, a Halo CME was identified by SOHO/LASCO on 09:36 UT with a linear plane-of-sky speed of 579 km/s. This CME was associated to a C6.6 solar flare from AR 12468 (S14° W02°) that peaked at 09:03 UT. Soon after, another Halo CME was spotted within the SOHO/LASCO field of view. This latter CME was slower with a linear plane-of-sky speed of 454 km/s and was marked on 14:24 UT. Figure 3 illustrates the relevant solar wind measurements from Wind, similar to Figure 1. The time span of the ICME was, again, obtained by the online repository http://www.srl.caltech.edu/ACE/ASC/DATA/level3/icmetable2.htm. The shock arrived at 1 AU on 19 December 2015 at 15:38 UT (see Table 1). At the same time, the second CME that was slower, propagated within interplanetary space. It is not clear if and how these two CMEs interacted during their travel from the Sun to the Earth. However, the in situ plasma data from Wind reveal more details. In particular, it seems that a few hours after the shock arrival the solar wind speed decreases, however it remains fairly stable within the ICME (ejecta) and began to gradually increase right after the crossing of the outer boundary of the ICME (see Table 1 and Figure 3). At the same time, the magnetic field remained relatively strong within the ICME (≈20nT) and was further sustained at almost 10 nT during the gradual increase of the solar wind speed. As concerns the evolution of the geomagnetic storm, the *D*$_{st}$ time profile (last panel of Figure 3) shows a two-step geomagnetic storm with a global minimum of −155 nT (orange vertical solid line). Following the shock arrival at 1 AU, and while into the sheath region the first drop of the *D*$_{st}$ index occurs. Once the boundary of the ICME is crossed, a second drop is identified in the *D*$_{st}$ time profile. The consequent crossing of the outer boundary of the ICME seems not to have a geomagnetic output. *B*$_Z$ became negative upon the crossing of the ICME and remained negative during the whole ejecta. Based on the aforementioned description, one could propose that the first CME resulted to an ICME and had a major role in the unfolding of the geomagnetic storm of 20 December 2015. However, it is not unprobable to suggest that the presence of two distinct CMEs that took place within hours had also a significant role in the evolution of the storm. In the case under consideration, the trailing CME is slower compared to the leading one. Usually, multiple CMEs result
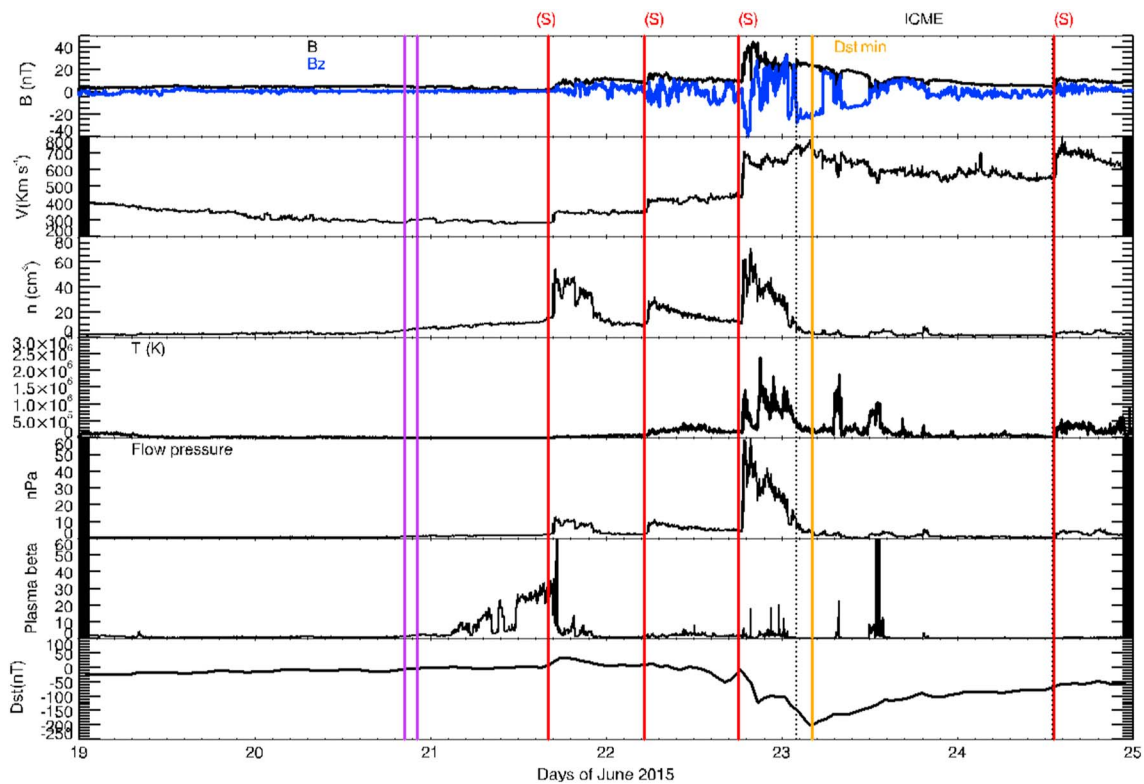
**Figure 2.** Similar to Figure 1 for the 23 June 2015 storm. Moreover, the two vertical purple lines correspond to the time window identified with critical behavior in the HellENIc GeoMagnetic Array time series (20 June 2015, 20:25–22:13 UT), that is, 45 hr prior to the peak of the storm (see also Figure 5).
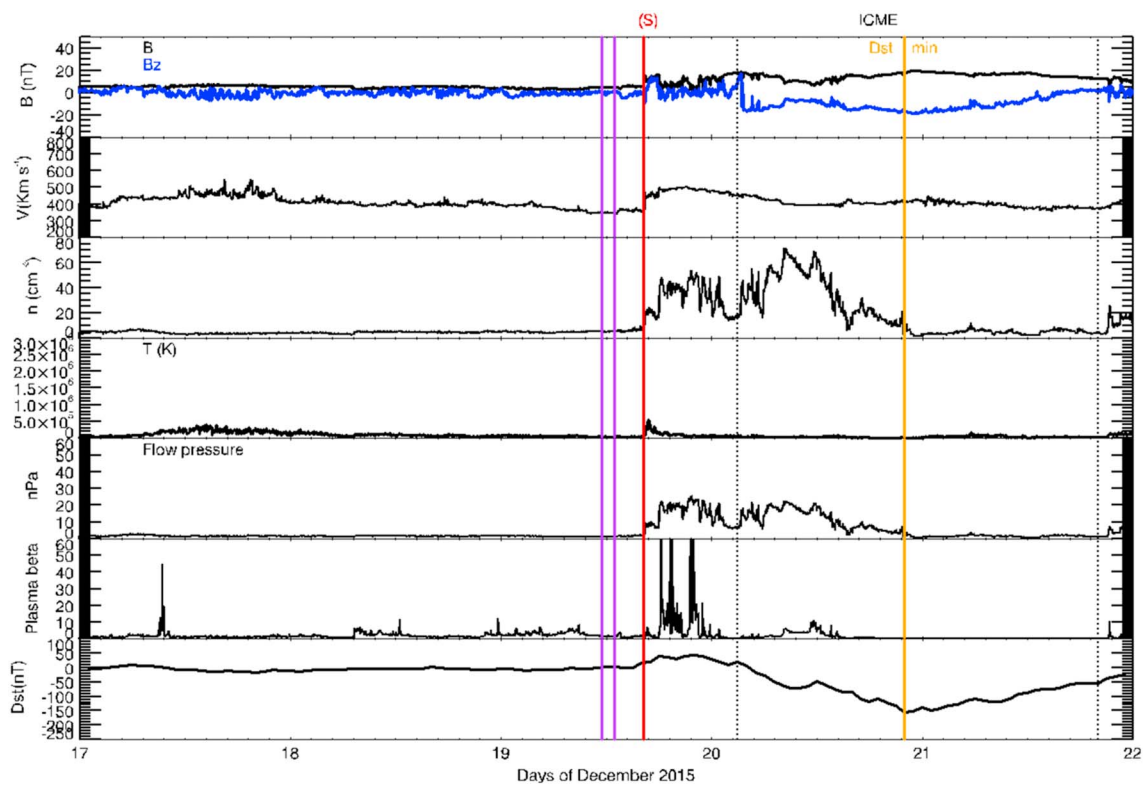


**Figure 3.** Similar to Figure 1 for the 20 December 2015 storm. Moreover, the two vertical purple lines correspond to the time window identified with critical behavior in the HellENIc GeoMagnetic Array time series (19 December 2015, 11:31–12:55 UT), that is, 6 hr prior to the peak of the storm (see also Figure 6).

to complex ejecta that tend to have a longer duration (than average) and thus drive the magnetosphere for an extended period (Lugaz & Farrugia, 2013); this could explain the gradual development of the geomagnetic storm and the long lasting ejecta.

## 3. The Method of Critical Fluctuations

The recently proposed method of critical fluctuations (MCF) has specifically been developed for the analysis of time series sourced from thermal systems governed by nonlinear intermittent dynamics (Contoyiannis & Diakonos, 2000; Contoyiannis et al., 2002). MCF is capable of identifying the existence of critical state, implying second-order phase transition in equilibrium, as well as the departure from it, while it has successfully been applied to a wide variety of dynamical systems ranging from theoretical thermal systems to geophysical, biological, electronic, and financial ones (Contoyiannis et al., 2002; Contoyiannis, Diakonos, Kapiris, et al., 2004; Contoyiannis, Diakonos, Papaefthimiou, & Theophilidis, 2004; Contoyiannis et al., 2015, 2016; Ozun et al., 2014; Potirakis et al., 2015, 2016, 2017, 2018). In the following we provide a brief presentation of the key theoretical aspects of MCF as well as a step-by-step procedure for its application to a time series. For a detailed study of the theoretical basis of MCF, the reader is referred to Contoyiannis and Diakonos (2000) and Contoyiannis et al. (2002, 2015).

It has been proposed by Contoyiannis and Diakonos (2000) that a nonlinear intermittent map of the form

$$\phi_{n+1} = \phi_n + u\phi_n^z \tag{1}$$

is capable of describing the dynamics of the fluctuations of the order parameter $\phi$ of a thermal system at critical state. In equation (1), $\phi_n$ is the $n$th sample of the scaled order parameter, $u > 0$ is a coupling parameter, and $z$ stands for a characteristic exponent associated with the isothermal exponent $\delta$ for critical systems at thermal equilibrium ($z = \delta + 1$). Actually, in order to more realistically model a real (or numerical) dynamical system one has to add a "noise" term, $\varepsilon_n$, to equation (1) (Contoyiannis & Diakonos, 2007), which, for positive values of the order parameter, becomes

$$\phi_{n+1} = \left| \phi_n + u\phi_n^z + \varepsilon_n \right|. \tag{2}$$

Note that in the special case of tricritical dynamics, the fluctuations of the order parameter $\phi$ have been proved (Contoyiannis et al., 2015) that can be expressed by a similar nonlinear intermittent map of the following form:

$$\phi_{n+1} = \left| \phi_n - u\phi_n^{-z} + \varepsilon_n \right| \tag{3}$$

The only difference between the maps of equations (2) and (3) is the opposite sign of both the coupling parameter and the characteristic exponent.

Criticality manifest itself by a power law distribution of properly defined laminar lengths (waiting times) $l$, $P(l) \sim l^{-p_l}$ (Schuster, 1998), where the exponent $p_l$ is directly related to the isothermal critical exponent $\delta$ as $p_l = 1 + 1/\delta \left[ = 1 + 1/(z+1) \right]$. However, as already mentioned in section 1, although criticality is always quantitatively manifested by power law, the vice versa is not valid, and power law is not necessarily sourced from critical dynamics. The key idea behind the MCF is that the analysis of a time series should not simply aim at the identification of a power law relation. On the contrary, a series of criticality characteristics should be step-by-step revealed for the specific time series before claiming that the underlying system is in critical state.

First of all, the time series excerpt under analysis should be checked for stationarity by requiring a nearly constant cumulative mean value with low corresponding standard deviation. Specifically, the evolution of the cumulative mean value and the corresponding standard deviation are estimated by starting the calculation using the first 500–1,000 values of the excerpt (depending on its total length) and progressively including more time series values in the calculation (usually by steps of 500–1,000 values). This check is necessary because criticality appears around a specific point of phase space (the critical point) during a second-order phase transition. Therefore, the implied gradual (smooth) change should manifest itself by, at least local, stationarity. The second characteristic concerns the values' distribution, which should present a flat maximum (plateau). Note that such a behavior can be attributed to the presence of a marginally stable fixed point (Schuster, 1998). If this scenario applies to the analyzed case, the plateau region can be considered as the immediate neighborhood of the fixed point (Contoyiannis & Diakonos, 2000; Diakonos & Schmelcher, 1997; Schmelcher & Diakonos, 1997). To determine whether the plateau region satisfies criticality, we calculate the distribution of the corresponding waiting times. The term "waiting times" denotes the number of successive time steps for which the analyzed time series trajectory belongs to the plateau. Contoyiannis et al. (2002)

showed that assuming that the origin of the plateau region is of critical character, the distribution of the corresponding waiting times follows power law with an exponent $p_l > 1$. Moreover, Contoyiannis et al. (2002) used the magnetization time series of the 3-D Ising model at the critical temperature to also show that the exponent $p_l$ can be associated with the isothermal critical exponent $\delta$ through the relation $p_l = 1 + 1/\delta$ (Schuster, 1998). To overcome the fact that the plateau region is not strictly defined, we assume a variable width of it and we perform a robustness check of our results with respect to small changes of the plateau width. Assuming that a power law with an exponent $p_l > 1$ is consistently identified regardless to these changes, then we assume that the time series indeed comes from a system in critical state. In previous works we have mentioned the plateau as "laminar region." Henceforth, we will use the term laminar region to denote the plateau of time series values distribution (see also the step-by-step procedure of MCF's application to a time series in the following).

A key step in the aforementioned reasoning is the check on whether the waiting times distribution follows power law along with the estimation of the power law exponent value. The function used in MCF to model the distribution of laminar lengths is (Contoyiannis & Diakonos, 2007):

$$f(l) = p_1 \cdot l^{-p_2} \cdot e^{-p_3 l}. \tag{4}$$

The experimentally determined waiting times distribution are fitted by equation (4) and the corresponding parameters $p_2$, $p_3$ are calculated. As shown in Contoyiannis et al. (2002) and Contoyiannis, Diakonos, Papaefthimiou, and Theophilidis (2004), this function deals with two important issues: (a) the finite size effects and (b) the distance from the critical point. We simulate both with the exponential factor $e^{-p_3 l}$ in equation (4). This term indicates the proximity to the critical point, if any, since it is dominant far away from criticality, while it becomes zero as we approach the critical point. When $p_3 = 0$ then the exponent $p_2$ in equation (4) should coincide with the abovementioned critical exponent $p_l$.

The two competitive terms of the function $f(l)$, the power law decay factor corresponding to critical dynamics, and the exponential decay factor describing memoryless, uncorrelated, noise, render possible to monitor the dynamics of the order parameter fluctuations. The critical dynamics as well as the departure from the critical state, either by the emergence of tricritical dynamics or by appearance of the so-called "symmetry breaking" phenomenon (will be explained later), can be identified. Note that equation (4) can efficiently model the distribution of laminar lengths in both cases of the nonlinear intermittent maps of equations (2) and (3) (Contoyiannis et al., 2015), which means that equation (4) can be used for the study of both kinds of dynamics. Specifically, the values of the $p_2$ (power law decay exponent) and $p_3$ (exponential decay exponent) signify the presence of critical dynamics or the departure from critical state in the following way:

1. $p_2 > 1$ and $p_3 \approx 0$ for a wide range of laminar regions imply predominance of critical dynamics, a second-order phase transition in equilibrium. The time series excerpt satisfying these criticality conditions is usually referred to as "critical window" (CW). Note that in this case, the approximation $p_l = p_2$ is valid, which means that $p_2$ has a clear physical interpretation through its relation to the abovementioned isothermal critical exponent $\delta$.
2. $p_2 < 1$ and $p_3 \approx 0$ for a wide range of laminar regions imply departure from the critical state by means of a tricritical crossover, that is, by passing from the second-order phase transition (high-symmetry state) to the first-order phase transition (low-symmetry state) through the vicinity of the tricritical point (an intermediate "mixing state").
3. Emergence of a bimodal distribution in the fluctuations of the order parameter is a first indication of possible departure from criticality. If the corresponding laminar lengths distribution can be fitted by equation (4) with $p_2 > 1$ and $p_3 \approx 0$ (critical signature) but only for a very narrow range of laminar regions (or even for just one laminar region), this is the signature of the theoretically expected so-called "symmetry breaking" phenomenon, signifying the transition from a highly symmetrical state (critical state), to a low-symmetry state, during which the process is focused around "preferred" directions. The marginal presence of power law distribution indicates that the system's state is still close to the critical point. The emergence of "symmetry breaking" after a CW indicates the departure from criticality.

The application of MCF comprises six simple steps:

1. Find a part of the time series with adequate length ($> \sim 5{,}000$ values) presenting, at least, local stationarity, by checking the cumulative mean value of the time series using nested time series excerpts of progressively wider length.

2. Calculate the histogram of the order parameter $\phi$ (which is usually the original time series values). Check the histogram for the presence of a flat maximum (plateau). If such a plateau is present, continue to the next step.

3. Determine a value from the histogram as the marginal unstable fixed-point $\phi_o$, which will serve as the "start of laminar regions." The marginal unstable fixed point in one-dimensional iterative maps like the map described by equation (2) is determined according to the turning point method (Diakonos & Schmelcher, 1997; Schmelcher & Diakonos, 1997). This usually lies at the abrupt edge of the histogram.

4. To ensure that the plateau region in the histogram of the order parameter $\phi$ is related to criticality, we have to calculate the distribution of the corresponding waiting times. For a number of different values within the $\phi$ amplitude range, which are called "ends of laminar regions" and denoted as $\phi_l$, calculate the distribution $P(l)$ of the laminar lengths of each corresponding laminar region $(\phi_o, \phi_l)$; one distribution per $\phi_l$ value. Laminar lengths are the waiting times within each laminar region $(\phi_o, \phi_l)$, in other words the number of successive $\phi$ values obeying the condition $\phi_o < \phi < \phi_l$. Note that all values within the $\phi$ amplitude range are examined as possible end points, while the examination is performed exhaustively by progressively increasing the number of equally spaced values covering the whole amplitude range. An empirical rule is checked before proceeding to the next step: the calculated distributions $P(l)$ should take nonzero values at least up to $l = 20 - 30$. If this rule is not satisfied, this means that it is necessary to add uniform noise as described in the next step (5) and then repeat steps (2)–(4), otherwise proceed to step (6).

5. If necessary (according to the criterion of step 4) add uniform noise in the range $[-\varepsilon_0, \varepsilon_0]$, with $\varepsilon_0$ of the order of $10^{-2}$ and repeat steps (2)–(4). The uniform noise is added after normalizing the original time series values of the time window under analysis in the range [0, 1], to numerically fit the problem to the nonlinear map of either equations (2) or (3). Consequently, the normalized time series values plus the uniform noise become the order parameter $\phi$ for the execution of steps (2)–(4). Note that for the nonlinear map of equation (2) with $z = 4$ within the range [0, 1] it has been found that the appropriate value was $\varepsilon_0 = 0.0175$ (Contoyiannis & Diakonos, 2007). However, for the case of real time series MCF steps (2)–(4) are initially applied directly to the original time series values with no addition of any noise ($\varepsilon_0 = 0$). But if the rule mentioned in step (4) is not satisfied, then an appropriate value of $\varepsilon_0 > 0$, of the order of $10^{-2}$, is determined by fine tuning and added to the normalized time series values before reexecuting steps (2)–(4).

6. Plot each one of the obtained distributions $P(l)$ on a log-log plot, and by fitting it using the function $f(l)$ of equation (4), determine a set of exponents $p_2, p_3$ for each laminar region. The dynamics are identified by the consistent behavior of the exponent values according to the cases (1)–(3) described above. In particular, as regards the range of end points for which the exponent values' conditions of cases (1) or (2) are satisfied, the wider the range is, the clearest the signature of criticality (case 1) or tricriticality (case 2) is.

## 4. Observation of Intermittency-Induced Criticality in Ground Magnetometer Time Series

In the following we present the analysis of the ground-based measurements of the geomagnetic field acquired around the three most intense magnetic storms of solar cycle 24, specifically the 17 March 2015 ($Dst_{min} = -223$ nT), 23 June 2015 ($Dst_{min} = -204$ nT), and 20 December 2015 ($Dst_{min} = -155$ nT) storms. We analyzed the unprocessed components ($X$, $Y$, and $Z$) of the geomagnetic field recorded at THL, DIO, and VLI stations (cf. http://enigma.space.noa.gr/) using the MCF time series analysis method. The analysis concerns a 5-day period for each storm, covering more than 3 days prior to the storm and the day including the peak of the storm. Figures 4–6 present the ENIGMA time series data analyzed in this study along with the Dst index time variations. Specifically, for the 17 March 2015 storm the time period 13–17 March 2015, while for the 23 June 2015 storm the time period 19–23 June 2015, as well as for the 20 December 2015 storm the period 16–20 December 2015, were analyzed.

The main objective was to investigate the possibility that one of the early stages of the preparation of the specific intense magnetic storms could present common characteristics with a thermal system undergoing a second-order phase transition. Specifically, we investigated, by means of the MCF, the possible existence of intermittency-induced critical dynamics in the small-scale (fast) variations of the abovementioned ground-based geomagnetic recordings during the quiet period a few days to a few hours prior to the onset of these events. As we show in the following, the application of MCF revealed that the intermittency-induced critical dynamics features were embedded in the geomagnetic data recorded prior to all three studied intense magnetic storm cases.
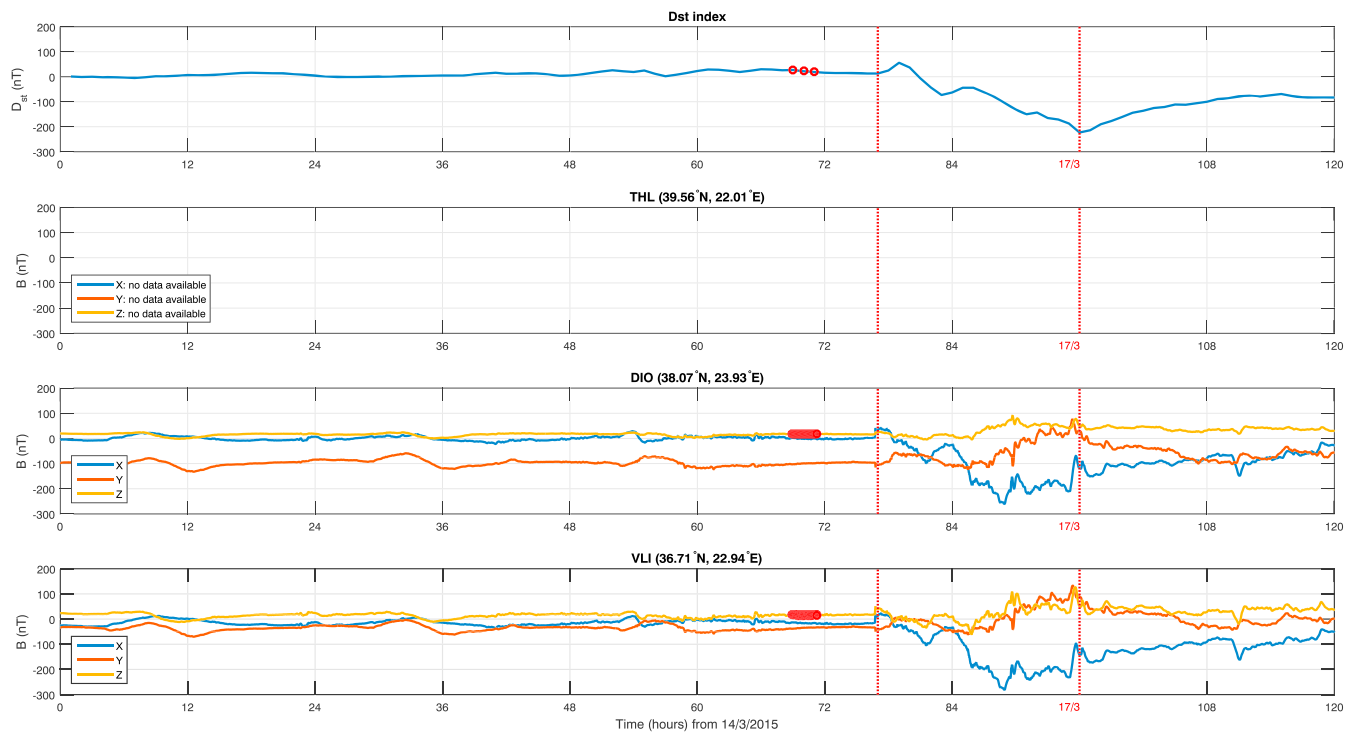
**Figure 4.** From top to bottom: The Dst index time variations along with the ENIGMA magnetic stations (ordered from north to south) geomagnetic field recordings *X*, *Y*, and *Z* during a period of 5 days for the 17 March 2015 storm. The interval of specific components of the DIO and VLI time series identified with critical behavior is marked in red. First and second red dashed lines denote the times of storm's onset and peak, respectively. (Please note that THL data are not available for 17 March 2015.)
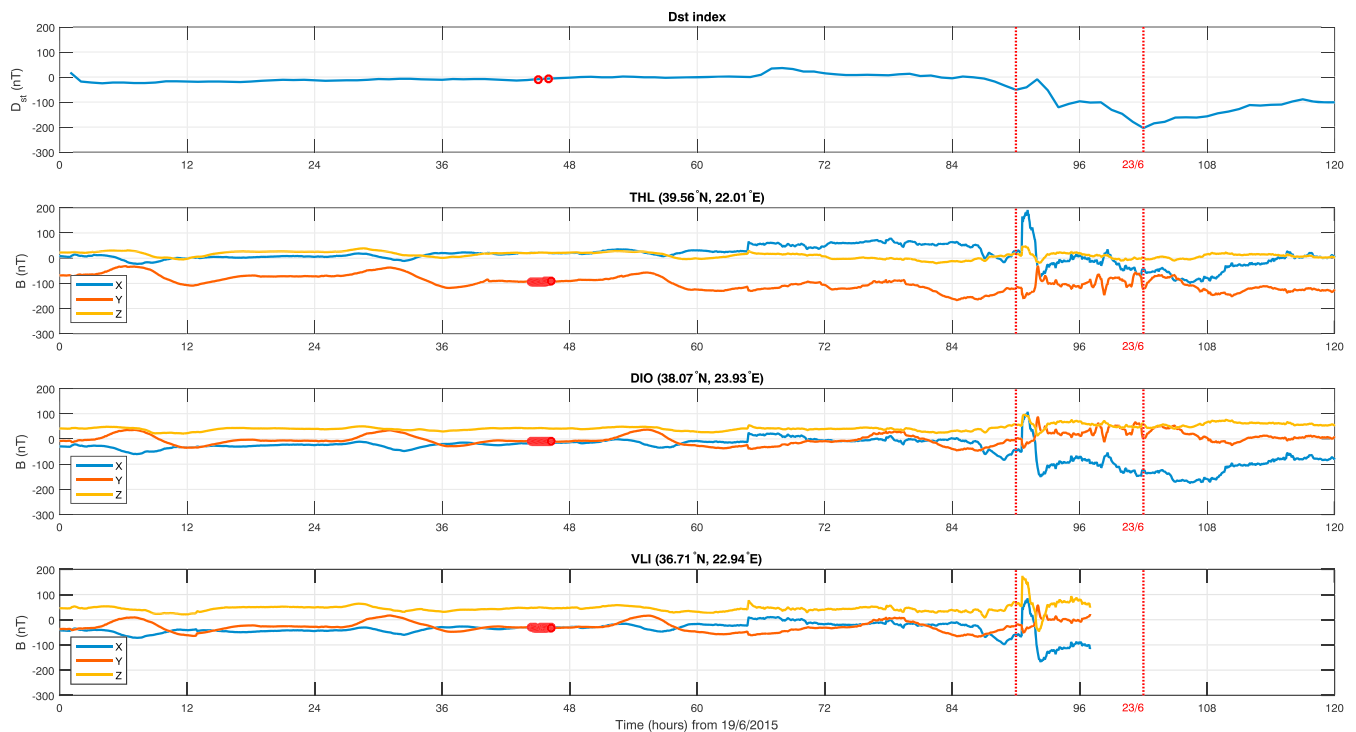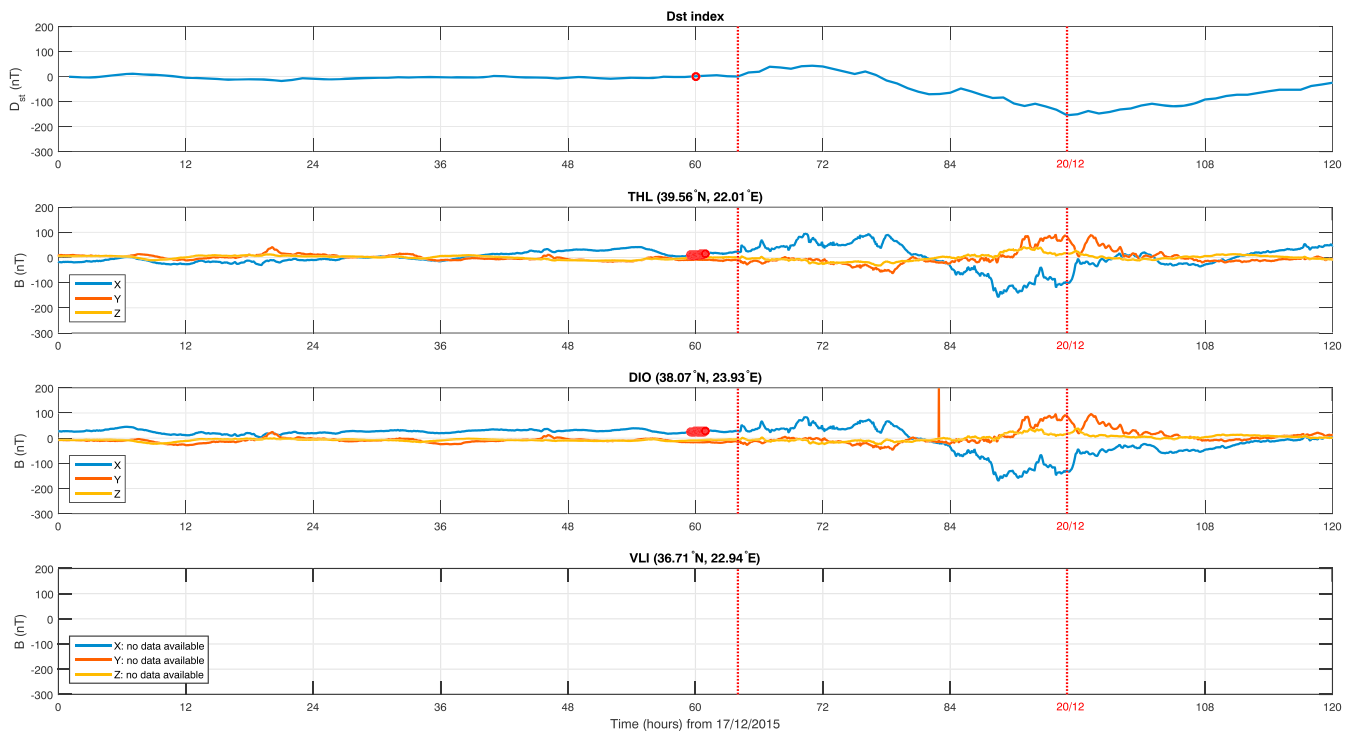


**Figure 5.** Similar to Figure 4 during a period of 5 days for the 23 June 2015 storm. The interval of specific components of the THL, DIO, and VLI time series identified with critical behavior are marked in red.

**Figure 6.** Similar to Figure 4 during a period of 5 days for the 20 December 2015 storm. The interval of specific components of the THL and DIO time series identified with critical behavior is marked in red. (Please note that VLI data are not available for 20 December 2015.)

We exhaustively applied, step-by-step, the six steps procedure for the application of MCF (see section 3) to the time series under analysis. First, we checked, according to MCF step (1), the $X$, $Y$, and $Z$ magnetic field time series searching for excerpts with adequate length ($> \sim 5{,}000$ values) presenting, at least, local stationarity, by calculating the cumulative mean value of the time series using nested time series excerpts of progressively wider length. As it has been recently discussed (Contoyiannis et al., 2016), the number of time series excerpts (or time windows) of the raw ground-based geomagnetic field measurements that present, at least locally, cumulative stationarity and thus can be analyzed through MCF is in general limited and the length of these time windows is relative narrow. The specific situation was verified once more in the case of the herein studied magnetic field observations. However, it was possible to find a number of time windows satisfying the abovementioned criteria. These time windows were further investigated by applying the next steps of MCF application procedure, searching for indications for the presence of critical dynamics or the departure from critical state according to the cases (1)–(3) described in section 3. Note that in applying the MCF procedure it was considered that the original time series values correspond to the order parameter $\phi$.

As described in section 3, MCF steps (2)–(4) were initially applied directly to the original time series values with no addition of any noise ($\varepsilon_0 = 0$). Our previous experience concerning the application of MCF on ground-based geomagnetic field recordings (Contoyiannis et al., 2016) showed that a certain amount of uniform noise (step (5), section 3) was usually necessary (according to the criterion of step (4), section 3) to be added. This should be "appropriately" selected so that it is high enough to lead to ergodicity but at the same time low enough in order not to mask the system dynamics. Indeed, this was also the case for the herein studied magnetic field time series. Therefore, in our case, after normalizing the time series in the range [0,1], an appropriate (determined by fine tuning) amount of uniform noise $[-\varepsilon_0, \varepsilon_0]$, with $\varepsilon_0$ of the order of $10^{-2}$, was added to the time windows revealed during MCF step (1) before further applying MCF analysis; this was capable of revealing the dynamics embedded in the studied time series (Contoyiannis & Diakonos, 2007). After that, according to the procedure presented in section 3, MCF steps (2)–(4) were repeated and then step (6) was applied.

An example demonstrating the main steps of MCF analysis is shown in Figure 7 for an excerpt of the DIO station recordings before the 23 June 2015 storm. Specifically, Figure 7a shows a 6,500 points long time window
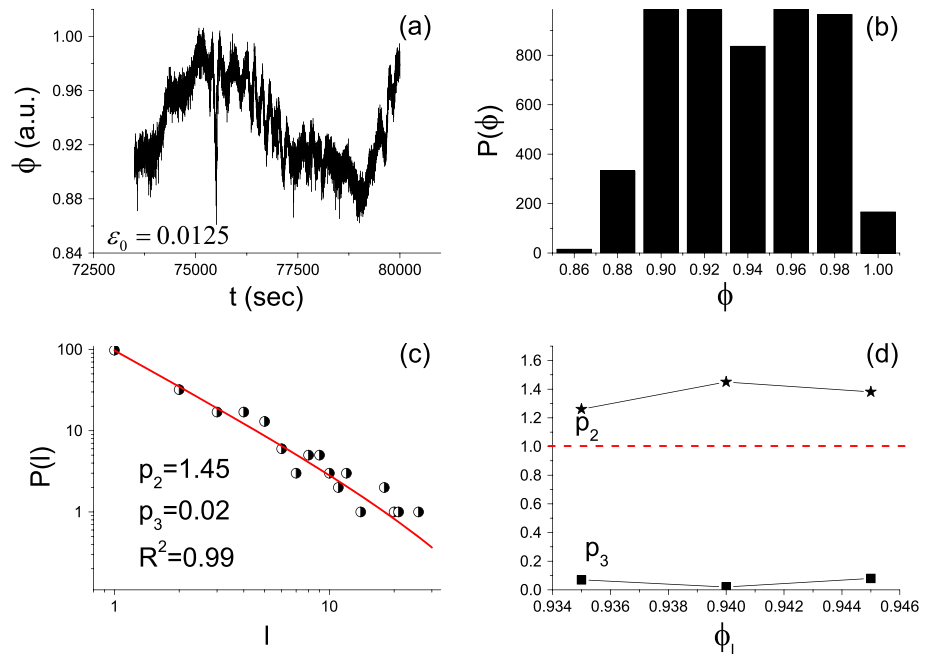
**Figure 7.** (a) A critical window of the 20 June 2015 DIO magnetic station recordings (after normalizing and adding uniform noise); the time scale refers to the time in seconds starting from 00:00:00 UT of the specific day. (b) The distribution of values for the time series of Figure 7a. (c) A representative example for laminar distribution, where the waiting times (laminar lengths) lie within 1 and 30 s. The continuous line corresponds to the fitted function of the form of equation (4), $f(l) \sim p_1 \cdot l^{-p_2} \cdot e^{-p_3 l}$, resulting to a set of exponents satisfying the conditions $p_2 > 1$ and $p_3 \approx 0$ of the case (1) described in section 3, which means that the power law factor of $f(l)$ is clearly dominating over the exponential one. It is noted that the use of $f(l)$ leads to good fitting results according to a number of popular goodness of fit parameters, while undoubtedly better compared with fitting by pure exponential function with a cutoff scale for example. (d) The exponents $[p_2, p_3]$ versus the end point $\phi_l$. The validity of criticality condition $[p_2 > 1, p_3 \approx 0]$ for a wide range of end point values (wide range of laminar regions) is clear.

of the $Y$ component of the geomagnetic field intensity after the normalization and addition of the necessary uniform noise in the range $[-0.0125, 0.0125]$. The specific time window was recorded on 20 June 2015, from 20:25:00 to 22:13:20 UT (cf. the time window marked by the vertical purple lines in Figure 2, as well as the part of the signal marked with thick red in Figure 5 for DIO station, second from bottom panel), that is, ~45 hr before the onset of the storm. As described in section 3, MCF steps (2)–(4) were applied after the normalization and addition of the abovementioned uniform noise. Figure 7b shows the histogram calculated during MCF step (2) for the order parameter $\phi$ (here the original time series values after normalization and addition of the necessary uniform noise) where the presence of an almost flat maximum can be identified in the histogram. Proceeding to MCF step (3), the marginal unstable fixed-point $\phi_0$, which will serve as the start of laminar regions, was determined from the histogram according to the turning point method (Diakonos & Schmelcher, 1997; Schmelcher & Diakonos, 1997) to be $\phi_0 = 0.88$. Next, we applied the MCF step (4), which means that we calculated the distribution $P(l)$ of the laminar lengths of the laminar region $(\phi_0, \phi_l)$, one distribution per $\phi_l$ (end of laminar regions) value, for a number of different values within the $\phi$ amplitude range. For each one of the obtained distributions $P(l)$, we proceeded, according to MCF step (6), to producing a log-log plot of $P(l)$ versus $l$, and by fitting it using the function $f(l)$ of equation (4), we determined a set of exponents $p_2, p_3$ for each laminar region. Figure 7c depicts, as an example, one such distribution with the obtained fitting and the corresponding exponents. Specifically, it shows the distribution $P(l)$ of the laminar lengths corresponding to the laminar region $(0.88, 0.94)$. Figure 7d shows the obtained sets of exponents for different laminar regions (i.e., the estimated $p_2, p_3$ versus the end of laminar regions, $\phi_l$ value). It can be observed that the conditions $p_2 > 1$ and $p_3 \approx 0$ are satisfied for a wide range of laminar regions that, according to the case (1) described in section 3, indicate predominance of intermittency-induced critical dynamics, implying a second-order phase transition in equilibrium. According to the MCF analysis, the time series excerpt under study is a CW.
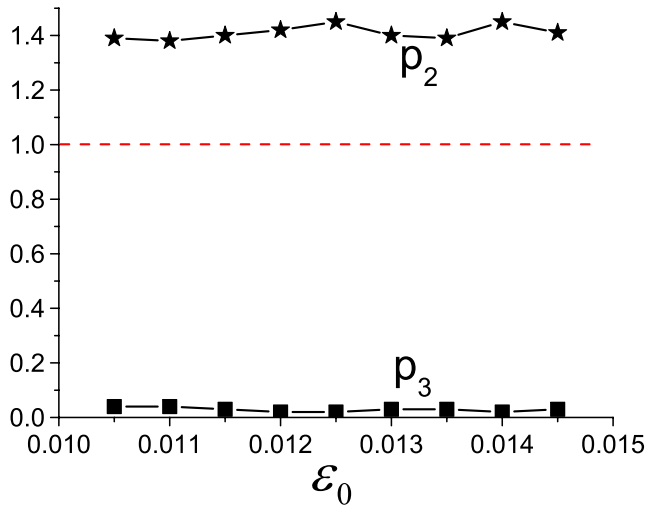
**Figure 8.** Dependence of the estimated values of the exponents $p_2$, $p_3$ on the change of the value of $\varepsilon_0$, for the laminar region corresponding to the representative example for laminar distribution shown in Figure 7c.

At this point we would like to clarify that the influence of the additional noise on the estimated values of the exponents $p_2$ and $p_3$ of the fitted function $f(l)$ of equation (4) is always tested in order to assure that these values do not change considerably upon a reasonable change of the amount of the added noise. As an example, we present in Figure 8 the change of exponents $p_2$ and $p_3$ of the fitted function $f(l)$ as a function of the added uniform noise $[-\varepsilon_0, \varepsilon_0]$ for the laminar distribution example shown in Figure 7c. As shown in Figure 8, the values of the exponents $p_2$ and $p_3$ are practically insensitive to the change of $\varepsilon_0$ value.

As shown in the above analyzed time series excerpt example, the stepwise MCF application procedure described in section 3 is by itself capable of uncovering the possible first-order nonlinear map dynamics embedded in a magnetic field time series identifying it as a CW. However, it is interesting to further investigate the properties of the specific CW of Figure 7a, by some independent means. For example, we can further verify the existence of such a correlation between time series values in many different ways, even though the dynamics cannot be determined in detail. Two possible ways are the study of the recurrence plot ($\phi_{n+1}$ versus $\phi_n$), as well as the autocorrelation function for two cases: (a) for the time series amplitude values as they were recorded and (b) after randomly shuffling the order of the recorded amplitude values. As shown in Figure 9 the recurrence plot of the recorded time series shows a clear distribution of values along the diagonal, implying the existence of first-order map dynamics, while this situation is dramatically changed after randomly shuffling the order of the recorded time series values. Shuffling results in the elimination of the dynamics and hence the random distribution of the points in the phase space. Moreover, Figure 10 clearly shows that the small-scale (fast) variations of recorded ground-based geomagnetic field measurements are strongly correlated, while this is destroyed after randomly shuffling the time series values. Consequently, it is obvious that the CW carries information which was possible to uncover by applying MCF. Note that by applying the MCF to the recorded time series values after randomly shuffling their order does not lead to any of the cases (1)–(3) described in section 3. This means that, as expected, no indication of specific dynamics was found by MCF for the randomly shuffled data.
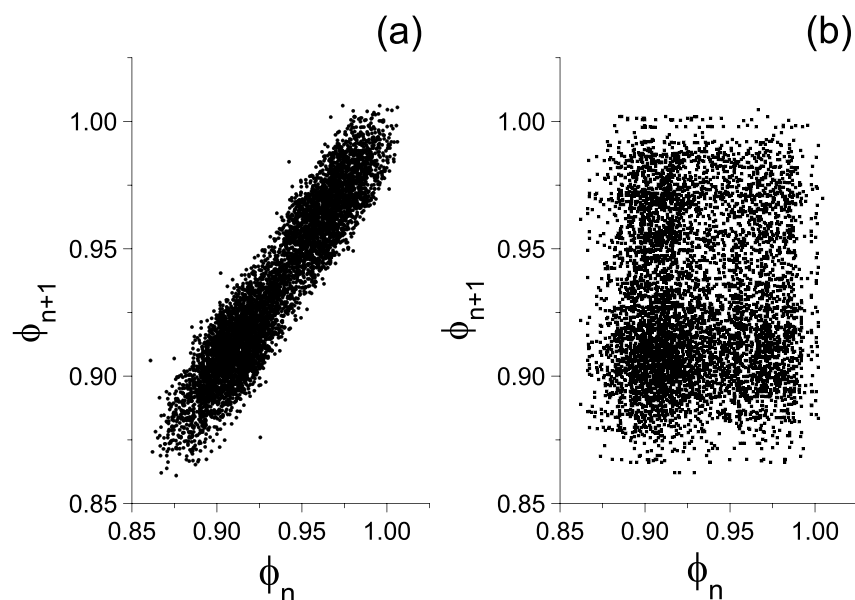


**Figure 9.** Recurrence plot of the critical window of Figure 7a. (a) Original $Y$ component of the geomagnetic field intensity (after normalizing and adding uniform noise) from DIO magnetic station on 20 June 2015. (b) The same time series (original values) after randomly shuffling their original order.
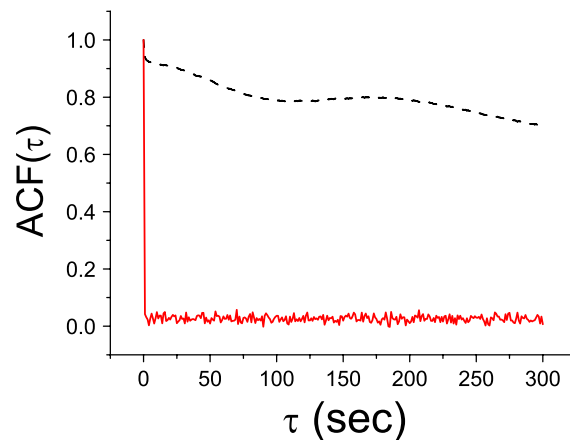
**Figure 10.** Autocorrelation function (ACF) plot for the critical window of Figure 7a (dashed curve, black), as well as for the same time series (original values) after randomly shuffling their original order (solid curve, red).

By exhaustively applying MCF on all possible candidate time windows of the $X$, $Y$, and $Z$ components of the magnetic field data under analysis on which the MCF could be applied (intervals of adequate length and stationarity) in summary, we found the following:

1. Concerning the 17 March 2015 storm and the correspondingly analyzed time period 13–17 March 2015:
    a. A CW of 8,500 samples was identified in the $Z$ component of the geomagnetic field recorded at DIO station on 16 March 2015 from 20:53:20 to 23:15:00 UT (cf. the time window marked by the vertical purple lines in Figure 1, as well as the part of the signal marked with thick red in Figure 4 for DIO station, second from bottom panel), that is, ~8 hr before the onset of the storm. During step (5) of the MCF analysis uniform noise in the range [−0.0125, 0.0125] was added. The specific time window, although yielded an excellent compliance to the condition $p_2 > 1$ and $p_3 \approx 0$ of the case (1) described in section 3, for example, $(p_2 = 1.47, p_3 = 0.06)|_{R^2=0.99}$, indicating intermittency-induced criticality, this happened only for a limited range of laminar regions.
    b. The same time window (16 March 2015 from 20:53:20 to 23:15:00 UT) of the $Z$ component recorded at VLI station exhibited critical behavior as well (cf. the time window marked by the vertical purple lines in Figure 1, as well as the part of the signal marked with thick red in Figure 4 for VLI station, bottom panel). Keeping the same added uniform noise as in the case of DIO $Z$ component, the fitting to equation (4) resulted to sets of exponents satisfying the conditions $p_2 > 1$ and $p_3 \approx 0$ of the case (1) described in section 3, for example, $(p_2 = 1.40, p_3 = 0.12)$. Although it is clearly $p_2 > 0$, $p_3$ is 1 order of magnitude higher than the corresponding calculated for the DIO critical time window. This result led us to the conclusion that VLI signal probably carries higher noise than the corresponding DIO one, and consequently, we probably need lower uniform noise to be added for achieving ergodicity. Indeed, after adding noise in the range [−0.007, 0.007] we found laminar lengths distributions clearly indicating intermittency-induced criticality, for example, $(p_2 = 1.68, p_3 = 0.03)|_{R^2=0.99}$.
    c. Unfortunately, THL station was inoperative during the analyzed time period related to the 17 March 2015 magnetic storm. Therefore, there are no analysis results for THL geomagnetic data.
    d. No criticality traces were found in the $X$ or the $Y$ components of the ground-based geomagnetic recordings of the ENIGMA network prior to the 17 March 2015 intense storm.
2. Regarding the 23 June 2015 storm and the corresponding time period 19–23 June 2015:
    a. A CW of 6,500 samples was identified in the DIO station recordings between 20:25:00 and 22:13:20 UT on 20 June 2015. The MCF analysis results for the specific time window have already been presented in detail earlier in this section and demonstrated in the form of Figures 7 and 8.
    b. During the same time window, intermittency-induced criticality was also revealed in the $Y$ component recordings of the VLI station (cf. the time window marked by the vertical purple lines in Figure 2, as well as the part of the signal marked with thick red in Figure 5 for VLI station, bottom panel), that is, ~45 hr before the onset of the storm. For additive uniform noise in the range [−0.005, 0.005] we were able to identify that the conditions $p_2 > 1$ and $p_3 \approx 0$, for example, $(p_2 = 1.73, p_3 = 0.01)|_{R^2=0.99}$, are satisfied indicating dynamics following the case (1) described in section 3.

**Table 2**
*Magnetic Local Times of the ENIGMA Magnetic Stations During the Three Intermittency-Induced Criticality (IIC) Events*

| No | Time interval of IIC event | THL station (39.57°N, 22.01°E, 86 m, $L = 1.47$) | DIO station (38.08°N, 23.93°E, 460 m, $L = 1.41$) | VLI station (36.72°N, 22.95°E, 220 m, $L = 1.35$) |
|---|---|---|---|---|
| 1 | 16/03/2015 (Z component) | | | |
| | 20:53:20–23:15:00 UT | Inoperative | MLT = 22.83– 1.16 | MLT = 22.74– 1.07 |
| 2 | 20/6/2015 (Y component) | | | |
| | 20:25:00–22:13:20 UT | MLT = 22.63– 0.46 | MLT = 22.73– 0.56 | MLT = 22.64– 0.47 |
| 3 | 19/12/2015 (X component) | | | |
| | 11:31:40–12:55:00 UT | MLT = 13.82–15.15 | MLT = 13.91–15.25 | Inoperative |

    c. The *Y* component recordings of THL station presented critical behavior as well during the same time window (cf. the time window marked by the vertical purple lines in Figure 2, as well as the part of the signal marked with thick red in Figure 5 for THL station, third from bottom panel). For uniform noise in the range [−0.007, 0.007] we found an excellent compliance to the conditions of the case (1) described in section 3, for example, $(p_2 = 1.42, p_3 = 0.06)\big|_{R^2=0.99}$, verifying the intermittency-induced critical behavior detected in the recordings of the other two observatories of ENIGMA network.

    d. No indications for criticality were found in the *X* or the *Z* components of the ground-based geomagnetic recordings of the ENIGMA network prior to the 23 June 2015 intense storm.

3. Concerning the 20 December 2015 storm and the correspondingly analyzed time period 16–20 December 2015:

    a. A CW of 5,000 samples was identified in the *X* component of the geomagnetic field recorded at DIO station on 19 December 2015 from 11:31:40 to 12:55:00 UT (cf. the time window marked by the vertical purple lines in Figure 3, as well as the part of the signal marked with thick red in Figure 6 for DIO station, second from bottom panel), that is, ~6 hr before the onset of the storm. After normalizing and adding uniform noise in the range [−0.0105, 0.0105] we found an excellent compliance to the conditions of the case (1) described in section 3, for example, $(p_2 = 1.80, p_3 = 0.025)\big|_{R^2=0.99}$, for a wide range of laminar regions which, according to the case (1) described in section 3, indicates predominance of intermittency-induced critical dynamics.

    b. The MCF analysis of the *X* component recordings of the THL station revealed intermittency-induced criticality during the same time window as in DIO station recordings (cf. the time window marked by the vertical purple lines in Figure 3, as well as the part of the signal marked with thick red in Figure 6 for THL station, third from bottom panel), that is, ~6 hr before the onset of the storm. By applying the MCF directly to the recorded values (no uniform noise was necessary to be added, that is, for $\varepsilon_0 = 0$), we were able to identify that the conditions $p_2 > 1$ and $p_3 \approx 0$, for example, $(p_2 = 1.67, p_3 = 0.012)\big|_{R^2=0.99}$, are satisfied indicating dynamics following the case (1) described in section 3.

    c. Unfortunately, VLI station was inoperative during the analyzed time period related to the 20 December 2015 magnetic storm. Therefore, there are no analysis results for VLI geomagnetic data.

    d. No indications for criticality were found in the *Y* or the *Z* components of the ground-based geomagnetic recordings of the ENIGMA network prior to the 20 December 2015 intense storm.

Table 2 summarizes the results and presents the MLTs of the ENIGMA magnetic stations when the intermittency-induced criticality events were observed along with the stations' geographic coordinates, altitudes and *L*-shell values. The stations are at midlatitudes, and their corresponding *L*-shell values range between approximately 1.3 and 1.5 $R_E$, which means that they are magnetically connected to the innermost boundary of the inner radiation belt (proton belt), which usually lies between *L* values 1 and 3 $R_E$.

Roldugin and Roldugin (2008) showed that the geomagnetic field variations, observed on the surface, are determined by Biot-Savart's law for a three-dimensional current system. Given the fact that the period identified with criticality for each magnetic storm was different (i.e., 8, 45, and 6 hr, respectively), it is reasonable to assume that these time differences would be reflected to different levels of variability for the external current system, which would in turn accompany the prestorm activity in each case. Therefore, for each storm

the corresponding differences in the variability of the external current system would be projected differently on the three components of the geomagnetic field on the ground.

## 5. Discussion and Conclusions

The geomagnetic field observations of the ENIGMA magnetometer array associated with the three most intense magnetic storms (Dst < −150 nT) of solar cycle 24, which occurred on 17 March 2015, 23 June 2015, and 20 December 2015, respectively, were analyzed in terms of the MCF time series analysis method, which has specifically been developed for the analysis of time series sourced from thermal systems governed by nonlinear intermittent dynamics. The application of the MCF analysis method on the unprocessed magnetic field variations ($X$, $Y$, and $Z$ components) provides evidence of the existence of intermittency-induced criticality 6, 8, and 45 hr prior the occurrence of the intense magnetic storms of December, March, and June 2015, respectively. Based on the obtained MCF analysis results, one could suggest that one of the early stages of the preparation of the specific intense magnetic storms presents common characteristics with a thermal system undergoing a second-order phase transition. Specifically, our results suggest the existence of intermittency-induced critical dynamics in the small-scale (fast) variations of the abovementioned ground-based geomagnetic recordings during the quiet period, that is, a few days to a few hours prior to the onset of the studied events. Despite the fact that the three intermittency-induced criticality events were observed prior to the occurrence of three intense magnetic storms a direct link between the critical fluctuations and the corresponding storm onset cannot be clearly established at this stage. However, the methodology shows promising capacity for the analysis of critical fluctuations in the framework of space systems.

We should note at this point that possible mechanisms of prestorm characteristics identified in data series have not been established, yet, since every magnetic storm carries its own characteristics. However, it has been suggested that the proton density of the solar wind prior to the occurrence of a geomagnetic storm may exhibit specific features that point to its arrival. This has been interpreted on the basis of density variability and increase that stimulates the release of energy accumulated in the magnetosphere. In particular, it has been found that the density of the solar wind is strongly correlated with the density of the plasma sheet (Borovsky et al., 1998), which, in turn, can be a driver of the ring current. Such features are identified several hours to days prior to geomagnetic storms (Khabarova et al., 2006). These findings are in principle in line with our observations: for these magnetic storms, the time interval that exhibits criticality features is closely related to the time period identified with prestorm features in the solar wind (see Figures 1–3 based on in situ plasma measurements from Wind (Lepping et al., 1995; Ogilvie et al., 1995)).

The first storm (March 2015) presented a two-step sequence, with the first minima identifying itself to the sheath region behind the shock, and the second one resulting from within the ICME. It is considered to be the output of an intense ICME. However, a recent study (Kataoka et al., 2015) employed a "pileup accident" hypothesis that brings together: (a) the fast CME/ICME—which is the main driver of the storm, (b) the HSS from a nearby coronal hole that followed the ICME, and (c) the preceding slow and high-density solar wind that was piled up ahead of the CME, to explain the unexpectedly geoeffective solar wind structure that gave ground to this intense storm. The second storm (June 2015) had a multistep development, caused by the southward fields due to amplification by a series of preceding shocks, resulting in the precondition of the magnetosphere that in turn fostered the growth of an intense geomagnetic storm (Liu et al., 2015; for more details on both storms see Marubashi et al., 2016, Wang et al., 2016, and Wu et al., 2016). The third storm (December 2015) presented a gradual structure that evolved within the boundaries (start to end time) of the ICME, while a southward field was present for the whole time interval, which, in turn, gave rise to this strong geomagnetic storm. However, it seems that this storm was driven by the possible interaction of two consecutive CMEs/ICMEs in the interplanetary space.

Assuming that the observed intermittency-induced criticality events are related to the magnetic storm events, the "warning" time range is most probably influenced by the degree of variability of each of the three cases. For instance, as concerns the first storm, simulations of corotating and transient solar wind disturbances (Figure 11) during this period show that the CME/ICME had the dominant role in the evolution of the geomagnetic storm with the preceding slow solar wind and the trailing HSS enhancing its complexity. Furthermore, solar wind density and $B_z$ variations are present almost a day before the arrival of the storm (see Figure 1). Such parameters have been identified as typical solar wind (prestorm) features prior to the occurrence
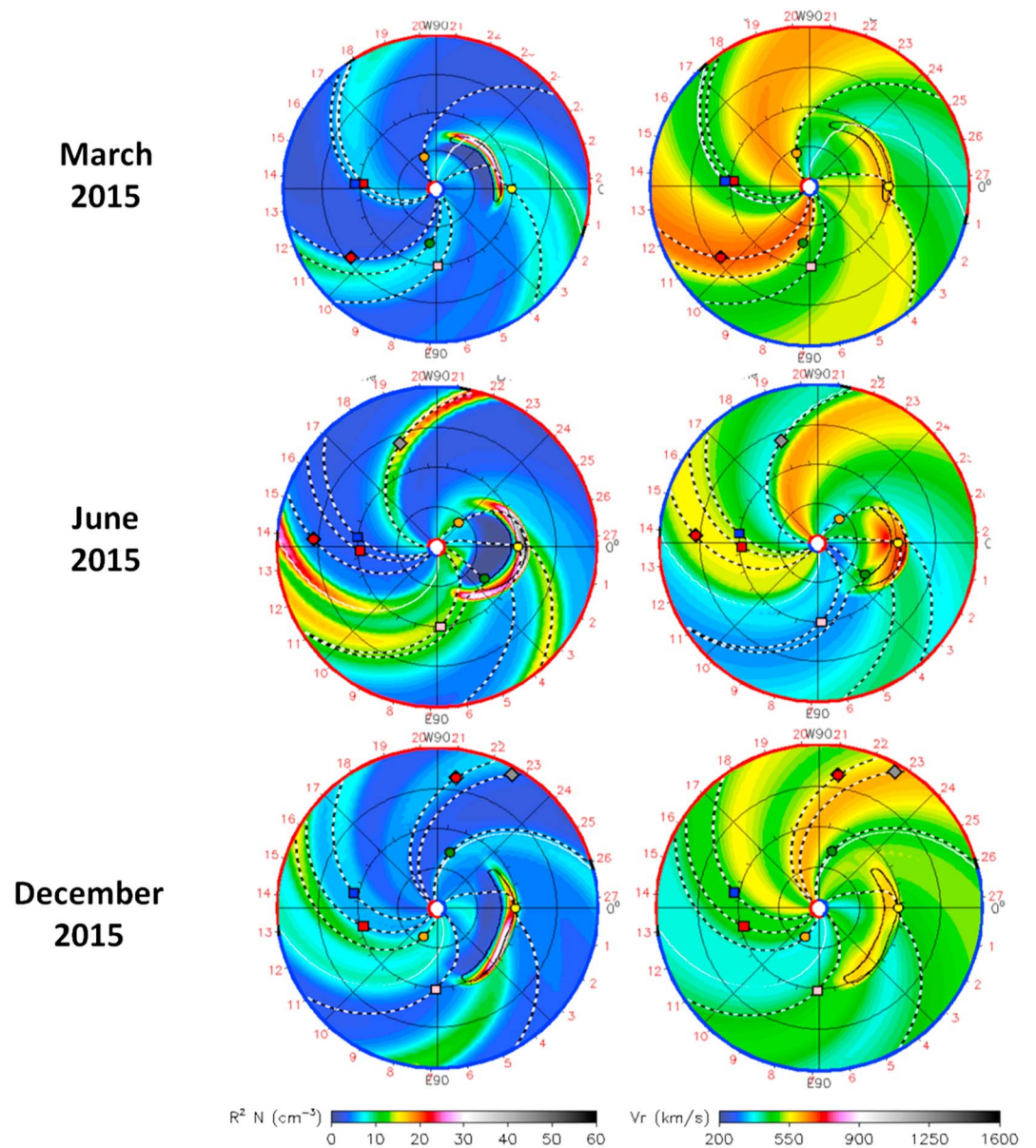
**Figure 11.** Simulations of the heliospheric environment using WSA+ENLIL, made available from the Space Weather Database Of Notifications, Knowledge, Information at https://ccmc.gsfc.nasa.gov/donki/. For each of the storms simulations on density (R; column on the left-hand side) and the velocity (Vr; column on the right-hand side) of the solar wind are presented.

of a geomagnetic storm (Khabarova et al., 2006). The period of criticality identifies itself right after the prestorm signatures and 8 hr before the actual onset of the storm (on March 17; Liu et al., 2015). The second storm exhibits a complex structure with multiple steps. As shown in a similar simulation (Figure 11) the sequence of CMEs/ICMEs fills the interplanetary (IP) space and drive shocks that clearly affect the geomagnetic conditions at Earth. The storm is the output of a series of strong and fast CMEs, while their corresponding IP shocks provide clear signatures in the in situ plasma and the ground-based geomagnetic field measurements (see Figure 2). In this case the period of criticality is spotted almost 45 hr in advance of the onset of the storm (on June 23; Liu et al., 2015). This period is also in agreement with moderate prestorm characteristics in the solar wind (Khabarova et al., 2006). Therefore, the preparatory phase and the intermittency-induced criticality are observed prior to the launch of the last CME of the series (see section 2), which resulted to the recorded geomagnetic storm. The third storm manifests a two-step structure. This storm is the output of the possible interaction of two consequent CMEs. Inspection of similar simulations (Figure 11) shows that these

CMEs (given their orientation) provide a wider CME front that encounters the Earth and results to this geomagnetic storm. In this case the period of criticality precedes the onset of the geomagnetic storm by about 6 hr and presents moderate prestorm characteristics in the solar wind (Khabarova et al., 2006).

Sitnov et al. (2001) suggested that magnetic storms may resemble features of first-order nonequilibrium transitions. Balasis et al. (2006, 2008) findings pointed to the appearance of two distinct patterns in the magnetosphere: (a) a pattern associated with the normal periods, which is characterized by a less ordered state or a lower degree of organization and (b) a pattern associated with the intense magnetic storms, which is characterized by a more ordered state or a higher degree of organization.

Criticality by intermittent dynamics was identified using the MCF during the quiet period a few days to a few hours prior to the onset of all three intense storms considered here. It is worth noting that the intermittency-induced criticality signatures reported in this article were simultaneously found in the recordings of all the stations of our network which were operating during the time period preceding each one of the magnetic storms of interest. We suggest that this implies that the identified critical dynamics could be related to a global phenomenon affecting geomagnetic field such as a magnetic storm. Intermittency-induced criticality dynamics imply a second-order phase transition in equilibrium. Our findings are compatible with the abovementioned suggestions. Specifically, criticality by intermittent dynamics correspond to the "normal" (quiet) period, it characterizes a state of the magnetosphere which precedes the dramatic change in magnetosphere dynamics, that is, the occurrence of the magnetic storm. In this context, it could be attributed to a distinct process that takes place during an early stage of the emergence of the ultimate extreme space weather phenomenon (magnetic storm).

The fact that a magnetic storm is a phenomenon out of equilibrium (an abrupt change analogous to a first-order phase transition) does not prevent its organization (an early stage of its preparation) to be accomplished by a mechanism in equilibrium conditions, such as the intermittency-induced criticality dynamics. At this early stage, the critical dynamics embedded in the observables' time series (here the ground-based geomagnetic field measurements) are found in time series excerpts with stationary characteristics. We clarify that we analyze only time series excerpts presenting, at least local, stationarity since it is expected that any observable of a system undergoing second-order transition in equilibrium should have stationary variation. In this regard, there is no point in analyzing parts of the geomagnetic field recordings just before or during a magnetic storm by means of the MCF. Moreover, it should be clarified that the organization of a critical process does not mean that the extreme phenomenon (the storm) will certainly fully evolve. Namely, if one can identify a critical state by analyzing the geomagnetic field time series, this does not necessarily mean that a magnetic storm will certainly follow. The revealed dynamics may evolve to the outburst of a storm or may not. Other precursory signs, following an identified criticality dynamics, such as the emergence of persistence dynamics or low complexity in the geomagnetic time series, are necessary before one could possibly suggest that a magnetic storm is inevitable.

In this work we used MCF to a posteriori investigate, whether specific magnetic storms were organized according to the aforementioned hypothesis. Namely, we investigated whether an intermittency-induced critical dynamics can be identified prior to the intense magnetic storms of March, June, and December 2015. After this early stage, when this organization is completed, out of equilibrium mechanisms could follow that may lead to the magnetic storm. Such mechanisms for the potential evolution from the early critical state (second-order phase transition) to the final storm state (first-order phase transition) might be the symmetry breaking or a tricritical crossover. Of course, at this point we cannot claim that the suggested early preparation stage can be identified for every magnetic storm. Much more cases should be analyzed in the future before attempting any generalization of our conclusions. In summary, the critical organization in stationary conditions, if this is found by the application of the MCF to the ground-based geomagnetic field measurements, could be an early indication of an upcoming magnetic storm. However, it should be clear that such a critical stage does not necessarily evolve to a magnetic storm. Such a precursor is not enough for the "safe" (the definite) prediction of a magnetic storm. In the future, following a more extended statistical analysis, space weather forecasting schemes could take into account these findings and implement them as potential precursory signatures of increased geomagnetic activity.

So far, the utilization of phase transition concepts and theory in treating space physics problems has been rather poor. Our results demonstrate that the mathematical framework of phase transitions can be used to represent the dynamics that govern the emergence of an extreme space weather phenomenon. Consequently,

we suggest that advanced prediction schemes of phase transition from other disciplines can be effectively applied for improving the capabilities of corresponding space weather prediction schemes.

## References

Angelopoulos, V., Mukai, T., & Kokubun, S. (1999). Evidence for intermittency in Earth's plasma sheet and implications for self-organized criticality. *Physics of Plasmas*, *6*, 4161–4168.

Baker, D. N., Klimas, A. J., McPherron, R. L., & Buchner, J. (1990). The evolution from weak to strong geomagnetic activity: An interpretation in terms of deterministic chaos. *Geophysical Research Letters*, *17*, 41–44.

Balasis, G., Daglis, I. A., Kapiris, P., Mandea, M., Vassiliadis, D., & Eftaxias, K. (2006). From pre-storm activity to magnetic storms: A transition described in terms of fractal dynamics. *Annales de Geophysique*, *24*, 3557–3567.

Balasis, G., Daglis, I. A., Papadimitriou, C., Kalimeri, M., Anastasiadis, A., & Eftaxias, K. (2008). Dynamical complexity in Dst time series using nonextensive Tsallis entropy. *Geophysical Research Letters*, *35*, L14102. https://doi.org/10.1029/2008GL034743

Balasis, G., Daglis, I. A., Papadimitriou, C., Kalimeri, M., Anastasiadis, A., & Eftaxias, K. (2009). Investigating dynamical complexity in the magnetosphere using various entropy measures. *Journal of Geophysical Research*, *114*, A00D06. https://doi.org/10.1029/2008JA014035

Borovsky, J. E., Thomsen, M. F., & Elphic, R. C. (1998). The driving of the plasma sheet by the solar wind. *Journal of Geophysical Research*, *103*(A8), 17,617–17,639. https://doi.org/10.1029/97JA02986

Chang, T. (1992). Low-dimensional behavior and symmetry breaking of stochastic systems near criticality-can these effects be observed in space and in the laboratory? *IEEE Transactions on Plasma Sciences*, *20*, 691–694.

Chapman, S. C., Watkins, N. W., Dendy, R. O., Helander, P., & Rowlands, G. (1998). A simple avalanche model as an analogue for the magnetospheric activity. *Geophysical Research Letters*, *25*, 2397–2400.

Consolini, G. (1997). Sandpile cellular automata and magnetospheric dynamics. In S. Aiello (Ed.), *Cosmic Physics in the Year 2000* (pp. 123–126). Bologna, Italy: SIF.

Consolini, G. (2002). Self-organized criticality: A new paradigm for the magnetotail dynamics. *Fractals*, *10*, 275–283.

Contoyiannis, Y. F., & Diakonos, F. K. (2000). Criticality and intermittency in the order parameter space. *Physics Letters A*, *268*, 286–292. https://doi.org/10.1016/S0375-9601(00)00180-8

Contoyiannis, Y. F., & Diakonos, F. K. (2007). Unimodal maps and order parameter fluctuations in the critical region. *Physical Review E*, *76*, 31138.

Contoyiannis, Y. F., Diakonos, F. K., Kapiris, P. G., Peratzakis, A. S., & Eftaxias, K. A. (2004). Intermittent dynamics of critical pre-seismic electromagnetic fluctuations. *Physics and Chemistry of the Earth*, *29*, 397–408. https://doi.org/10.1016/j.pce.2003.11.012

Contoyiannis, Y. F., Diakonos, F. K., & Malakis, A. (2002). Intermittent dynamics of critical fluctuations. *Physical Review Letters*, *89*, 35701. https://doi.org/10.1103/PhysRevLett.89.035701

Contoyiannis, Y. F., Diakonos, F. K., Papaefthimiou, C., & Theophilidis, G. (2004). Criticality in the relaxation phase of a spontaneously contracting atria isolated from a Frog's Heart. *Physical Review Letters*, *93*, 98101. https://doi.org/10.1103/PhysRevLett.93.098101

Contoyiannis, Y. F., Potirakis, S. M., Eftaxias, K., & Contoyianni, L. (2015). Tricritical crossover in earthquake preparation by analyzing preseismic electromagnetic emissions. *Journal of Geodynamics*, *84*, 40–54. https://doi.org/10.1016/j.jog.2014.09.015

Contoyiannis, Y. F., Potirakis, S. M., Eftaxias, K., Hayakawa, M., & Schekotov, A. (2016). Intermittent criticality revealed in ULF magnetic fields prior to the 11 March 2011 Tohoku earthquake (Mw = 9). *Physica A*, *452*, 19–28. https://doi.org/10.1016/j.physa.2016.01.065

Daglis, I. (2001). The storm-time ring current. *Space Science Reviews*, *98*, 343–363.

Diakonos, F. K., & Schmelcher, P. (1997). Turning point properties as a method for the characterization of the ergodic dynamics of one-dimensional iterative maps. *Chaos*, *7*(2), 239–244. https://doi.org/10.1063/1.166249

Freeman, M. P., Watkins, N. W., & Riley, D. J. (2000). Power law distributions of burst duration and interburst interval in the solar wind: Turbulence or dissipative self-organized criticality? *Physical Review E*, *62*, 8794–8797.

Gjerloev, J. W. (2009). A global ground-based magnetometer initiative. *EOS*, *90*, 230–231. https://doi.org/10. 1029/2009EO270002

Gonzalez, W. D., Tsurutani, B. T., & Clu'a de Gonzalez, A. L. (1999). Interplanetary origin of geomagnetic storms. *Space Science Reviews*, *88*, 529–562.

Gopalswamy, N., Akiyama, S., Yashiro, S., Xie, H., Makela, P., & Michalek, G. (2015). The mild space weather of solar cycle 24. In *Proc. 14th Int. Ionospheric Effects Symp* (pp. 79–86). Alexandria, VA, 12-14 May 2015. Retrieved from https://arxiv.org/abs/1508.01603

Gosling, J. T., McComas, D. J., Phillips, J. L., & Bame, S. J. (1991). Geomagnetic activity associated with Earth passage of interplanetary shock disturbances and coronal mass ejections. *Journal of Geophysical Research*, *96*, 7831–7839.

Huang, K. (1987). *Statistical mechanics* (2nd ed). New York: John Wiley.

Kataoka, R., Shiota, D., Kilpua, E., & Keika, K. (2015). Pileup accident hypothesis of magnetic storm on 17 March 2015. *Geophysical Research Letters*, *42*, 5155–5161. https://doi.org/10.1002/2015GL064816

Khabarova, O., Pilipenko, V., Engebretson, M. J., & Rudenchik, E. (2006). Solar wind and interplanetary magnetic field features before magnetic storm onset. *Proceedings of International Conference of Substorms*, *8*, 1–6.

Klimas, A. J., Vassiliadis, D., Baker, D. N., & Roberts, D. A. (1996). The organized nonlinear dynamics of the magnetosphere. *Journal of Geophysical Research*, *101*, 13,089–13,113.

Lepping, R. P., Acūna, M. H., Burlaga, L. F., Farrell, W. M., Slavin, J. A., Schatten, K. H., et al. (1995). The WIND magnetic field investigation. *Space Science Reviews*, *71*, 207–229. https://doi.org/10.1007/BF00751330

Liu, Y. D., Huidong, H., Wang, R., Yang, Z., Zhu, B., Liu, Y. A., et al. (2015). Plasma and magnetic field characteristics of solar coronal mass ejections in relation to geomagnetic storm intensity and variability. *The Astrophysical Journal Letters*, *809*, L34. https://doi.org/10.1088/2041-8205/809/2/L34

Lugaz, N., & Farrugia, C. J. (2013). A new class of complex ejecta resulting from the interaction of two coronal mass ejections with different orientations and its expected geo-effectiveness. *Geophysical Research Letters*, *41*, 769–776. https://doi.org/10.1002/2013GL058789

Lui, A. T. Y., Chapman, S. C., Liou, K., Newell, P. T., Meng, C. I., Brittnacher, M., & Parks, G. K. (2000). Is the dynamic magnetosphere an avalanching system? *Geophysical Research Letters*, *27*, 911–914.

Marubashi, K., Cho, K.-S., Kim, R.-S., Kim, S., Park, S.-H., & Ishibashi, H. (2016). The 17 March 2015 storm: The associated magnetic flux rope structure and the storm development. *Earth, Planets and Space*, *68*, 173. https://doi.org/10.1186/s40623-016-0551-9

Ogilvie, K. W., Chornay, D. J., Fritzenreiter, R. J., Hunsaker, F., Keller, J., Lobell, J., et al. (1995). WE, a comprehensive plasma instrument for the WIND spacecraft. *Space Science Reviews*, *71*, 55–77. https://doi.org/10.1007/BF00751326

Ozun, A., Contoyiannis, Y. F., Diakonos, F. K., Hanias, M., & Magafas, L. (2014). Intermittency in stock market dynamic. *Journal of Trading*, *9*(3), 26–33.

Pesnell, W. D. (2016). Predictions of solar cycle 24: How are we doing? *Space Weather*, *14*, 10–21. https://doi.org/10.1002/2015SW001304

Potirakis, S. M., Contoyiannis, Y., Asano, T., & Hayakawa, M. (2018). Intermittency-induced criticality in the lower ionosphere prior to the 2016 Kumamoto earthquakes as embedded in the VLF propagation data observed at multiple stations. *Tectonophysics*, *722*, 422–431. https://doi.org/10.1016/j.tecto.2017.11.020

Potirakis, S. M., Contoyiannis, Y., Diakonos, F. K., & Hanias, M. P. (2017). Intermittency-induced criticality in a resistor-inductor-diode circuit. *Physical Review E*, *95*, 42206. https://doi.org/10.1103/PhysRevE.95.042206

Potirakis, S. M., Contoyiannis, Y., Eftaxias, K., Koulouras, G., & Nomicos, C. (2015). Recent field observations indicating an Earth system in critical condition before the occurrence of a significant earthquake. *IEEE Geoscience and Remote Sensing Letters*, *12*(3), 631–635. https://doi.org/10.1109/LGRS.2014.2354374

Potirakis, S. M., Contoyiannis, Y., Melis, N. S., Kopanas, J., Antonopoulos, G., Balasis, G., et al. (2016). Recent seismic activity at Cephalonia (Greece): A study through candidate electromagnetic precursors in terms of non-linear dynamics. *Nonlinear Processes in Geophysics*, *23*, 223–240. https://doi.org/10.5194/npg-23-223-2016

Roldugin, V. C., & Roldugin, A. V. (2008). Pc5 pulsations on the ground, in the magnetosphere, and in the electron precipitation: Event of 19 January 2005. *Journal of Geophysical Research*, *113*, A04222. https://doi.org/10.1029/2007JA012553

Schmelcher, P., & Diakonos, F. K. (1997). A turning point analysis of the ergodic dynamics of iterative maps. *International Journal of Bifurcation and Chaos*, *7*(11), 2459. https://doi.org/10.1142/S0218127497001643

Schuster, H. (1998). *Deterministic Chaos*. Weinheim: VCH.

Sharma, A. S., Vassiliadis, D., & Papadopoulos, K. (1993). Reconstruction of low-dimensional magnetospheric dynamics by singular spectrum analysis. *Geophysical Research Letters*, *20*, 335–338.

Sitnov, M. I., Sharma, A. S., Papadopoulos, K., & Vassiliadis, D. (2001). Modeling substorm dynamics of the magnetosphere: From self-organization and self-organized criticality to nonequilibrium phase transitions. *Physical Review E*, *65*, 16116. https://doi.org/10.1103/PhysRevE.65.016116

Sornette, D. (2004). *Critical phenomena in natural sciences*. Heidelberg, Germany: Springer.

Stanley, H. E. (1987). *Introduction to phase transitions and critical phenomena*. New York: Oxford University Press.

Stanley, H. E. (1999). Scaling, universality, and renormalization: Three pillars of modern critical phenomena. *Reviews of Modern Physics*, *71*, S358–S366.

Tsurutani, B., Sugiura, M., Iyemori, T., Goldstein, B., Gonzalez, W., Akasofu, A., & Smith, E. (1990). The nonlinear response of AE to the IMF BS driver: A spectral break at 5 hours. *Geophysical Research Letters*, *17*, 279–282.

Uritsky, V. M., & Pudovkin, M. I. (1998). Low frequency 1 = f-like fluctuations of the AE-index as a possible manifestation of self-organized criticality in the magnetosphere. *Annales de Geophysique*, *16*, 1580–1588.

Vassiliadis, D. V., Sharma, A. S., Eastman, T. E., & Papadopoulos, K. (1990). Low-dimensional chaos in magnetospheric activity from AE time series. *Geophysical Research Letters*, *17*, 1841–1844.

Vörös, Z., Baumjohann, W., Nakamura, R., Runov, A., Zhang, T. L., Volwerk, M., et al. (2003). Multi-scale magnetic field intermittence in the plasma sheet. *Annales de Geophysique*, *21*, 1955–1964.

Wang, Y., Zhang, Q., Liu, J., Shen, C., Shen, F., Yang, Z., et al. (2016). On the propagation of a geoeffective coronal mass ejection during 15–17 March 2015. *Journal of Geophysical Research: Space Physics*, *121*, 7423–7434. https://doi.org/10.1002/2016JA022924

Wanliss, J. (2005). Fractal properties of SYM-H during quiet and active times. *Journal of Geophysical Research*, *110*, A03202. https://doi.org/10.1029/2004JA010544

Wanliss, J. A., & Dobias, P. (2007). Space storm as a dynamic phase transition. *Journal of Atmospheric and Solar-Terrestrial Physics*, *69*, 675–684.

Watari, S. (2017). Geomagnetic storms of cycle 24 and their solar sources. *Earth, Planets and Space*, *69*, 70. https://doi.org/10.1186/s40623-017-0653-z

Wu, C. C., Liou, K., Lepping, R. P., Hutting, L., Plunkett, S., Howard, R. A., & Socker, D. (2016). The first super geomagnetic storm of solar cycle 24: "The St. Patrick's day event (17 March 2015)". *Earth, Planets and Space*, *68*, 151. https://doi.org/10.1186/s40623-016-0525-y